Research Article

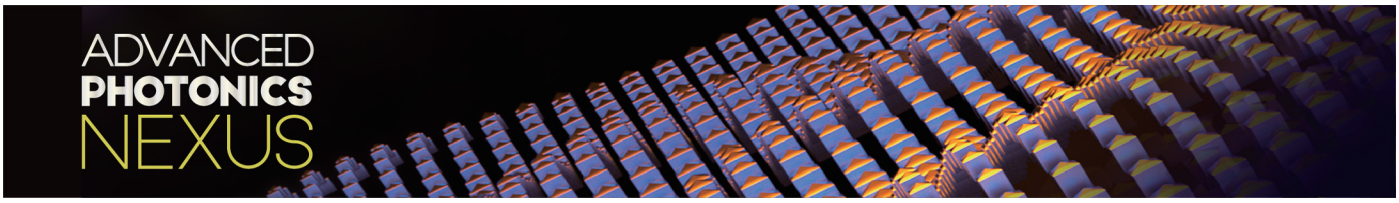

Arbitrary hybrid and higher-order Poincaré sphere beam generation by metasurfaces via a unified design framework

Chuang Sun,[a] Hailong Pi,[a] Kian Shen Kiang,[a] Jun-Yu Ou,[b,*] and Jize Yan[a,*]
[a]University of Southampton, School of Electronics and Computer Science, Southampton, United Kingdom
[b]University of Southampton, School of Physics and Astronomy, Southampton, United Kingdom

Abstract. The unique phase profile and polarization distribution of the vector vortex beam (VVB) have been a subject of increasing interest in classical and quantum optics. The development of higher-order Poincaré sphere (HOPS) and hybrid-order Poincaré sphere (HyOPS) has provided a systematic description of VVB. However, the generation of arbitrary VVBs on a HOPS and a HyOPS via a metasurface lacks a unified design framework, despite numerous reported approaches. We present a unified design framework incorporating all design parameters (e.g., focal lengths and orders) of arbitrary HOPS and HyOPS beams into a single equation. In proof-of-concept experiments, we experimentally demonstrated four metasurfaces to generate arbitrary beams on the fifth-order HOPS (nonfocused and tightly focused, NA 0.89), 0-2 order, and 0-1 order HyOPS. We showed HOPS beams' propagation and focusing properties, the superresolution focusing characteristics of the first-order cylindrical VVBs, and the different focusing properties of integer-order and fractional-order cylindrical VVBs. The simplicity and feasibility of the proposed design framework make it a potential catalyst for arbitrary VVBs using metasurfaces in applications of optical imaging, communication, and optical trapping.

Keywords: metasurface; vector vortex beam; Poincaré sphere.

Received Aug. 26, 2024; revised manuscript received Nov. 12, 2024; accepted for publication Dec. 23, 2024; published online Feb. 17, 2025.

[DOI: 10.1117/1.APN.4.1.016015]

1 Introduction

Structured light beams are attracting researchers' attention in many research fields because of their powerful application potential in classic and quantum fields ranging from laser communication, superresolution imaging, and lithography, to multidimensional optical manipulation.[1–5] The vector vortex beam (VVB), as a special group of structured light beams, has a spatially inhomogeneous state of polarization (SOP) and phase profile on its cross section that makes it carry orbital angular momentum (OAM) and spin angular momentum (SAM).[6]

A theoretical framework named higher-order Poincaré sphere (HOPS) is developed to describe the VVB's total angular momentum and the evolution of its SOP and phase profile, which provides researchers with great utility and convenience in studying the VVB.[7] The two poles of HOPS represent two scalar vortex beams with spatially homogenous SOP [i.e., left circular polarization (LCP) and right circular polarization (RCP)] and vortex phase profile, which possesses an SAM of $\sigma\hbar$ ($\sigma = \pm 1$) and an OAM of $l\hbar$ (l is the orders of a HOPS and the topological charge of a vortex beam).[6,7] The equator of a HOPS represents a set of cylindrical vector beams that carry no angular momentum and is a widely used type of VVB because of its superresolution imaging and lithography capability.[3,4,6]

Constrained by the identical angular momentum carried by the HOPS beams, their applicability remains limited to specific scenarios.[8] The hybrid-order Poincaré sphere (HyOPS) is developed to broaden the scope of HOPS to a more general form, where the left- and right-circular polarization beams represented by the northern and southern poles have distinct topological

*Address all correspondence to Jun-Yu Ou, bruce.ou@soton.ac.uk; Jize Yan, J.Yan@soton.ac.uk

charges ($|\ell_{\mathrm{LCP}}| \neq |\ell_{\mathrm{RCP}}|$). As a result, the total angular momentum carried by a HyOPS beam varies across its surface.[9] Conventionally, HOPS and HyOPS beams can be generated by introducing a bulky anisotropic crystal, q plate, spiral phase plate, and spatial light modulator (SLM) to an optical path.[1,4,6] For instance, the HOPS can be generated in a multicore fiber amplifier by shaping the seed laser beam via an SLM.[9] In addition, the SLM is also used for generating the multidimensional structured light described by the SU (2) Poincaré sphere.[10–13]

Based on the generalized Fresnel theorem and abrupt phase induced by a subwavelength meta-atom,[14] the metasurface, which is composed of an array of subwavelength meta-atoms on a flat substrate, is capable of engineering incoming light's amplitude, phase, and polarization.[15–19] Furthermore, metasurface is lightweight, low cost, capable of mass production, scaled up, and capable of integrating with an on-chip light source (e.g., a vertical-cavity surface-emitting laser).[20,21] Therefore, many design approaches have been developed for generating and focusing the cylindrical vector beams, HOPS beams, and HyOPS beams.[22–34] Compared with the plasmonic-based metasurface, the all-dielectric metasurface attracts intensive attention because it can avoid ohmic losses and realize high manipulation efficiency. Its fabrication requires only a single-step lithography and is complementary metal–oxide–semiconductor (CMOS)-compatible.[15] Till now, there has been no unified theoretical framework to design single-layer all-dielectric metasurfaces for controlled generating unfocused and focused VVBs on a HOPS or a HyOPS. In addition, the HOPS and HyOPS beams have not been experimentally generated by metasurfaces in the wavelength of 1550 nm, even though this wavelength plays an essential role in laser communication, biological imaging, and optical manipulation.[21,35]

In this paper, the target phase profiles from the fundamental definition for generating arbitrary nonfocused/focused VVBs on HOPS and HyOPS are derived. A unified design framework of an all-dielectric metasurface for generating nonfocused/focused VVBs on a HOPS and HyOPS is proposed in Sec. 3, and the controlled generation principle of the arbitrary VVB over the HOPS and HyOPS is analyzed. In Sec. 4, we design, fabricate, and characterize four metasurface samples working in the wavelength of 1550 nm to generate arbitrary VVBs on the fifth-order HOPS (nonfocused and tightly focused), 0-2 order HyOPS, and 0-1 order HyOPS. The experimental results agree well with the theoretical expectation values, showcasing the unified design framework's feasibility and potential applications.

2 Phase Profiles for Generating HOPS and HyOPS Beams

Figure 1 shows a fundamental Poincaré sphere (FPS) [Fig. 1(a)], a HOPS [Fig. 1(b)], and a HyOPS [Fig. 1(c)]. Arbitrary VVBs on a HyOPS can be expressed as Eq. (1), where α is the azimuthal angle in the polar coordinate of the light beam's cross section, $\tilde{A}_{\mathrm{LN}} = A_{\mathrm{LN}} e^{i(\varphi_{\mathrm{LN}})}$ and $\tilde{A}_{\mathrm{RM}} = A_{\mathrm{RM}} e^{i(\varphi_{\mathrm{RM}})}$ are the complex amplitudes of the LCP $\left(\text{i.e., } |L\rangle = \frac{\sqrt{2}}{2}\begin{bmatrix} 1 \\ i \end{bmatrix}\right)$ vortex component with a topological charge of N and the RCP $\left(\text{i.e., } |R\rangle = \frac{\sqrt{2}}{2}\begin{bmatrix} 1 \\ -i \end{bmatrix}\right)$ vortex component with a topological charge of M.[8] Note that N should not be equal to M for the HyOPS beams:,

$$U = A_{\mathrm{LN}} e^{i(\varphi_{\mathrm{LN}})} e^{i(N\alpha)} |L\rangle + A_{\mathrm{RM}} e^{i(\varphi_{\mathrm{RM}})} e^{i(M\alpha)} |R\rangle. \tag{1}$$

From Eq. (1), the VVBs on a HyOPS combine two orthogonal LCP and RCP vortex components with different topological charges. As shown in Fig. 1(c), from the northern pole to the southern pole of a HyOPS, Eq. (1) could vary from a scalar plane beam to a scalar vortex beam with a topologic charge of 2 by setting $M = 0$ and $N = 2$. The equator of the HyOPS represents a set of cylindrical VVBs, where the LCP and RCP components have the same amplitudes, $A_{\mathrm{LN}} = A_{\mathrm{RM}}$.

The scalar beams on the FPS [Fig. 1(a)] have a uniform polarization distribution overall in the beam's cross section and Gaussian intensity distribution. When $N = M = 0$, Eq. (1) is simplified to Eq. (2), which describes all the scalar beams on the FPS. Therefore, the arbitrary polarization state of a scalar beam can be decomposed into two orthogonal LCP and RCP components. The polarization states would vary with the complex amplitudes $\tilde{A}_{\mathrm{LN}}$ and $\tilde{A}_{\mathrm{RM}}$. Specifically, the LCP and RCP components in a linear polarization (LP) light

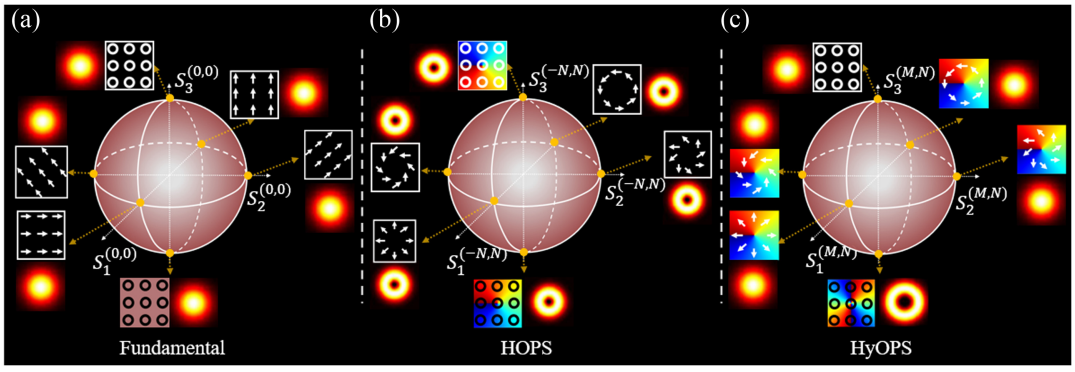

Fig. 1 (a) FPS, (b) HOPS, and (c) HyOPS. $S_1^{(N,M)}$, $S_2^{(N,M)}$, and $S_3^{(N,M)}$ are the Stokes parameters of the beams, and the superscript (M, N) denotes the topological charges carried by the LCP (southern pole) and RCP (northern pole) beams. When $M = -N$, the LCP and RCP beams are vortex beams of the same topological charge with opposite signs, and the HyOPS (c) is degraded to the HOPS (b). Moreover, when $M = N = 0$, the LCP and RCP beams are plane waves, and the HOPS is degraded to an FPS (a).

beam have the same amplitudes $A_{\mathrm{LN}} = A_{\mathrm{RM}}$, and the phase difference $\Delta\varphi_{\mathrm{RL}} = \varphi_{\mathrm{RM}} - \varphi_{\mathrm{LN}}$ determines the polarization direction of an LP laser beam,[7] illustrated by the FPS equator in Fig. 1(a). In experimental constructions, arbitrary scalar beams on an FPS can be obtained by combining a quarter-wave plate (QWP) and a half-wave plate (HWP). In other words, $\tilde{A}_{\mathrm{LN}}$ and $\tilde{A}_{\mathrm{RM}}$ can be easily tuned to arbitrary values via a QWP and an HWP,

$$U = \tilde{A}_{\mathrm{LN}}|L\rangle + \tilde{A}_{\mathrm{RM}}|R\rangle. \tag{2}$$

As shown in Fig. 1(b), the light beams on a HOPS have a spatially varied distribution in phase and polarization. In addition, the orthogonal LCP and RCP components in a HOPS beam are vortex beams having the same topological charge N with opposite signs. Therefore, Eq. (1) can be rewritten into Eq. (3) for describing the HOPS beams by replacing M with $-N$. According to Fig. 1(b) and Eq. (3), the equator of a HOPS represents a set of cylindrical vector beams with an order of $N-1$. Two special cases (azimuthal and radial vector beams) of cylindrical vector beams are widely used for superresolution imaging and lithography because of their unique focusing performance, which will be demonstrated in Sec. 4,

$$U = \tilde{A}_{\mathrm{LN}}e^{i(N\alpha)}|L\rangle + \tilde{A}_{\mathrm{RM}}e^{i(-N\alpha)}|R\rangle. \tag{3}$$

Based on the relationship among the FPS, HOPS, and HyOPS [i.e., Eqs. (1)–(3)], a unity design framework can be proposed to generate arbitrary VVBs on HOPS and HyOPS via an all-dielectric metasurface. However, no focusing phase is included in Eq. (1). A hyperbolic focusing phase profile is needed to obtain arbitrary focused VVBs. Equation (4) should be imparted to the LCP and RCP components in Eq. (1),[16]

$$\Phi(\rho, f) = \frac{2\pi}{\lambda}\left(f - \sqrt{f^2 + \rho^2}\right), \tag{4}$$

$$U(\rho,\alpha) = e^{i\left[\Phi(\rho)+\left(\frac{N+M}{2}\right)\alpha\right]}\left\{\tilde{A}_{LN}e^{i\left(\frac{N-M}{2}\alpha\right)}|L\rangle + \tilde{A}_{\mathrm{RM}}e^{i\left(\frac{M-N}{2}\alpha\right)}|R\rangle\right\}. \tag{5}$$

In Eq. (4), ρ is the radius of the light beam's cross section. Introducing Eq. (4) into Eq. (1), arbitrary focused VVBs can be expressed as Eq. (5), which indicates that the critical function of the dielectric metasurface would be to impart the polarization-independent phase profile of $\Phi(\rho) + (\frac{N+M}{2})\alpha$ and polarization-dependent phase profile of $\pm(\frac{N-M}{2}\alpha)$ onto an incoming scalar LP beam. To clarify the unified design framework via Eq. (5), Secs. S1 and S2 in the Supplementary Material derived the working mechanism of a dielectric metasurface and provided a general design flow, respectively.

3 Dielectric Metasurface for Generating Arbitrary PS Beams

3.1 Metasurface Design

As discussed in Sec. 2, the metasurface needs to impart a propagation phase profile Ψ^{PP} [Eq. (6)] and a geometry phase profile Ψ^{GP} [Eq. (7)] to the transmitted light beam. Based on the meta-atom library built up in Sec. S2 in the Supplementary Material, the metasurface can be designed following a general flow, as shown in Fig. 2(a),

$$\Psi^{\mathrm{PP}}(\rho,\ \alpha) = \Phi(\rho, f) + \left(\frac{N+M}{2}\right)\alpha, \tag{6}$$

$$\Psi^{\mathrm{GP}}(\rho,\ \alpha) = \pm\left(\frac{N-M}{2}\alpha\right). \tag{7}$$

Taking the metasurface of generating arbitrary focused VVBs on a HyOPS ($M = 0$, $N = 2$, and NA = 0.89) as an

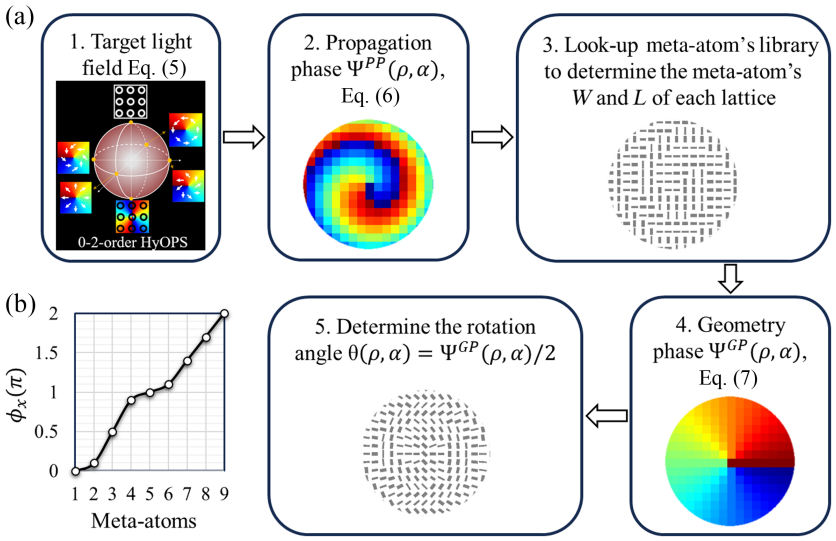

Fig. 2 (a) Design flow and (b) meta-atom's library of the dielectric metasurface for generating HOPS and HyOPS beams.

example, Fig. 2(a) demonstrates the metasurface design flow in detail. Starting from the digitalization of the target propagation phase $\Psi^{PP}(\rho,\alpha)$, we can first determine the meta-atom's dimensions (W, L) at each lattice by looking up the meta-atom's library [Fig. 2(b)]. Next, the required geometry phase profile [Eq. (7)] and the rotation angle $\theta(\rho,\alpha)=\Psi^{GP}(\rho,\alpha)/2$ at each lattice can be determined. As a result, the rotation angle of the meta-atom array owns a distribution of $\theta(\rho,\alpha)=(N-M)\alpha/4$.

3.2 Manipulating the Transmitted Light over the Whole PS Surface

A set of QWP and HWP is adopted to manipulate the transmitted light over the whole PS surface to achieve arbitrary VVBs on a target HOPS or HyOPS [Fig. 3(a)]. An LP light beam (E_γ in Fig. 3, the polarization direction γ) passing through the QWP and HWP can be described as U_0 [Eq. (8)] based on the Jones matrix,

$$U_0=\begin{bmatrix}\cos(2\chi) & \sin(2\chi)\\ \sin(2\chi) & -\cos(2\chi)\end{bmatrix}\begin{bmatrix}1 & 0\\ 0 & i\end{bmatrix}\begin{bmatrix}\cos(\gamma)\\ \sin(\gamma)\end{bmatrix}, \tag{8}$$

$$\begin{cases}\tilde{A}_{LN}=\frac{1}{\sqrt{2}}[\cos(\gamma)+\sin(\gamma)]e^{i(2\chi)}\\ \tilde{A}_{RM}=\frac{1}{\sqrt{2}}[\cos(\gamma)-\sin(\gamma)]e^{i(-2\chi)}\end{cases}. \tag{9}$$

To determine the polarization U_0 (i.e., the polarization angles 2ϑ and 2ψ on an FPS), the complex amplitudes $\tilde{A}_{LN}$ and $\tilde{A}_{RM}$ [Eq. (9) as well as in Eq. (2)] of the LCP and RCP components in U_0 need to be obtained first. Substituting $\tilde{A}_{LN}$ and $\tilde{A}_{RM}$ into the definition of Stokes parameters, we can obtain the position angles (2ϑ and 2ψ in Fig. 3) [Eq. (10)],

$$\begin{cases}2\psi=-4\chi\\ 2\vartheta=-2\gamma\end{cases}. \tag{10}$$

In Eq. (10), as well as in the Stokes parameters, 2ψ denotes the phase difference between the RCP and LCP components. As both χ and γ angles can be continuously tuned from 0 to 2π, arbitrary values of 2ψ and 2ϑ (i.e., $\tilde{A}_{LN}$ and $\tilde{A}_{RM}$) can be obtained. Therefore, a set of HWP and QWP can achieve arbitrary beams represented by an FPS.

Substituting Eqs. (6), (7), and (9) into Eq. (S5) in the Supplementary Material, the light beam passing through the metasurface sample can be obtained as Eq. (11), which demonstrates arbitrary VVBs on a specific HOPS and HyOPS. As shown in Figs. 3(b) and 3(c), after passing through the metasurface, the light beam's position on a HOPS and HyOPS would be opposite to its position on the FPS because the LCP (RCP) component is converted to be RCP (LCP) component by the metasurface [Eqs. (9) and (11)],

$$\begin{bmatrix}E_x^o\\ E_y^o\end{bmatrix}=e^{i\left[\Phi(\rho)+\left(\frac{N+M}{2}\right)\alpha\right]}\left\{\frac{1}{\sqrt{2}}[\cos(\gamma)-\sin(\gamma)]e^{i(-2\chi)}e^{i\left(\frac{N-M}{2}\alpha\right)}|L\rangle+\right.$$
$$\left.\ldots\frac{1}{\sqrt{2}}[\cos(\gamma)+\sin(\gamma)]e^{i(2\chi)}e^{i\left(\frac{M-N}{2}\alpha\right)}|R\rangle\right\}. \tag{11}$$

Specifically, when $\gamma=0$ (i.e., the polarization direction of the incoming light is along the SA of the QWP), 2ϑ equal to zeros [Eq. (10)] as well. It means that, for $\gamma=0$, Eq. (11) represents the vector beams on the equator of the HOPS and HyOPS. Introducing $\gamma=0$ into Eq. (8), the outgoing light beam $U_0(\gamma=0)=\begin{bmatrix}\cos(2\chi)\\ \sin(2\chi)\end{bmatrix}$, which is LP and has a polarization direction $\beta=2\chi$. Substituting $\beta=2\chi$, $\theta(\rho,\alpha)=(N-M)\alpha/4$, and Eq. (6) into Eq. (S9) in the Supplementary Material, we

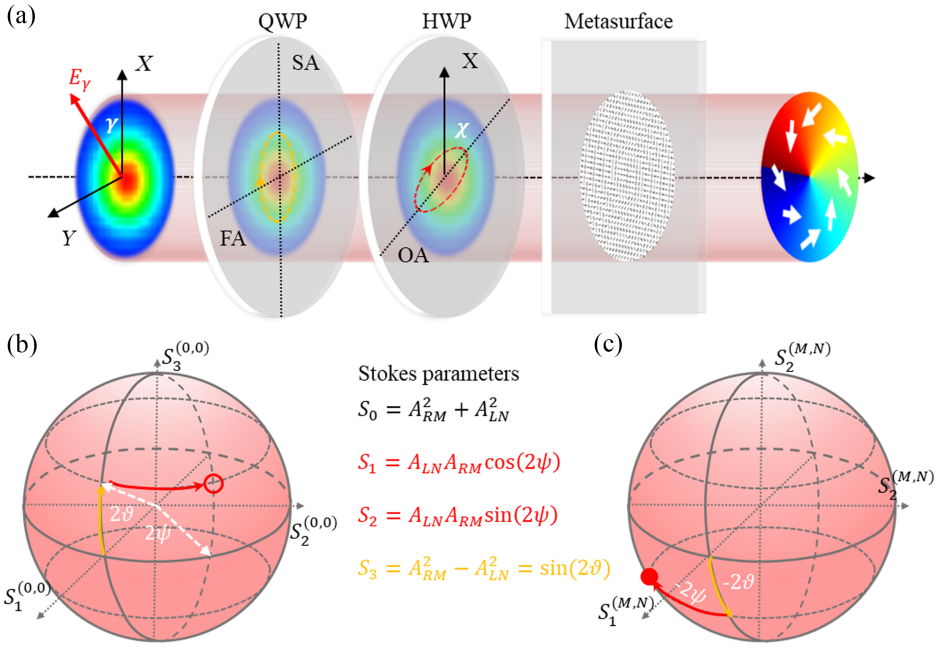

Fig. 3 (a) Scheme of generating arbitrary VVBs on a target HOPS or HyOPS. (b) The circular point represents a scalar beam having a position angle $(2\vartheta, 2\psi)$. (c) The solid red point is the transmitted light beam's position $(-2\vartheta, -2\psi)$ on a HOPS/HyOPS.

Table 1 Parameters and target of metasurface samples.

Number of samples	Design parameter	Target
1	$M = 5$, $N = -5$, $\Phi(\rho) = 0$	Nonfocused fifth-order HOPS beams
2	$M = 5$, $N = -5$, $f = 300\ \mu$m	Focused fifth-order HOPS beams (NA = 0.89)
3	$M = 0$, $N = 2$, $f = 1$ mm	Focused 0-2 order HyOPS beams (NA = 0.89)
4	$M = 0$, $N = 1$, $f = 1$ mm	Focused 0-1 order HyOPS beams (NA = 0.89)

can obtain the light beam transmitted from the metasurface [Eq. (12)]. Equation (12) demonstrates that the vector beams represented by the HOPS and HyOPS' equator are a set of cylindrical VVBs with an order of $(N-M)/2$ and a topological charge of $(N+M)/2$. For example, when $N = 2$, $M = 0$, the equator represents a set of cylindrical VVBs with an order of 1 and a topological charge of 1, as shown in Figs. 1(c) and 3(a). Although Eq. (12) agrees with Eq. (11), based on an LP basis, Eq. (12) gives a clearer and simpler description of the cylindrical VVBs represented by the equator,

$$\begin{bmatrix} E_x^o \\ E_y^o \end{bmatrix}_{\gamma=0} = e^{i\left[\Phi(\rho)+\left(\frac{N+M}{2}\right)\alpha\right]} \begin{bmatrix} \cos\left[\frac{(N-M)\alpha}{2} - 2\chi\right] \\ \sin\left[\frac{(N-M)\alpha}{2} - 2\chi\right] \end{bmatrix}. \tag{12}$$

We have derived the unified design framework and generation mechanism of arbitrary vector beams on a HOPS/HyOPS. Specifically, based on the LP basis, we give a quantitative value of the cylindrical VVBs represented by a HOPS/HyOPS' equator. Four proof-of-concept experiments are operated in Sec. 4, where four metasurface samples are used with customized functions (i.e., design parameters). The design parameters and target function of the four samples are summarized in Table 1.

4 Proof-of-Concept Experiments

4.1 Generation of Nonfocused Fifth-Order HOPS Beams

The metasurface sample 1 is first designed by setting $M = 5$, $N = -5$, and $\Phi(\rho) = 0$ to generate arbitrary nonfocused fifth-order HOPS beams. The intensity distribution of the transmitted light beam is theoretically calculated based on Eq. (11) and illustrated in Fig. 4(a). The position angles $(2\vartheta, 2\psi)$ in Fig. 4(a) are obtained based on Eq. (10) and the parameters (γ, χ) adopted for Eq. (11). Considering the orthogonality of the X and Y components in the transmitted light and the symmetry of the X and Y component's intensity, Fig. 4(a) only depicts the near field of the X component in the transmitted light beam. As shown in Fig. 4(a), the near-field distribution of the X component becomes a gear-like pattern from an almost uniform pattern by manipulating 2ϑ from $\pm\frac{\pi}{2}$ to 0. (i.e., the transmitted light beam $\begin{bmatrix} E_x^o \\ E_y^o \end{bmatrix}$ is manipulated from the two poles to the equator).

In the experiment, the transmitted light beam $\begin{bmatrix} E_x^o \\ E_y^o \end{bmatrix}$ is collected via a customized microscope where sample 1 is illuminated by a collimated 1550 nm laser beam. To obtain the near-field distribution of the X component, the microscope is focused on sample 1 ($Z = 0$), and a polarizer is placed in front of the camera to select the X component in the transmitted light beam. Figure 4(b) shows the experiment result where the near field of the X component is tuned to be a clearly gear-like pattern from an almost uniform pattern by manipulating 2γ (i.e., -2ϑ) from $-\frac{\pi}{2}$ to 0.

Based on the Fourier transformation of the near field, the far field of the X component is obtained and shown in Fig. 4(a) as well. The distribution of the near field and far field of the transmitted light beam is quite different, as shown in Fig. 4(a). Therefore, it is meaningful to figure out how the transmitted light beam evolves from the near-field pattern ($Z = 0$) to the far-field pattern. Keeping $\gamma = 0$ $(2\vartheta = 0)$, the intensity evolution with the propagation distance Z is theoretically obtained via angular spectrum theory[27] and measured in the experiment. The theoretical and experimental results are shown in Figs. 4(c1) and 4(c2), respectively. Our experimental results coincide well with the theoretical results. From both numerical and experimental results, the gear-like near field ($Z = 0$ mm) gradually converges to the expected far-field pattern with multiple lobes at around $Z = 12$ mm, and then the far-field pattern becomes divergent ($Z > 12$ mm).

4.2 Generation of Tightly Focused Fifth-Order HOPS Beams

To obtain the tightly focused fifth-order HOPS beams via the metasurface, the metasurface sample 2, with a diameter of 1.2 mm, is designed by setting $M = 5$, $N = -5$, and $f = 300\ \mu$m. The target NA of sample 2 is 0.89. The tightly focused far field (Fig. 5) is measured at the focal plane of sample 2.

Figure 5 demonstrates the controlled generation of tightly focused fifth-order HOPS beams along its longitude line and equator by tuning the angles (γ, χ). It could be seen that the far field of X and Y components is orthogonal to each, and the total fields are donut-shaped over the whole fifth-order HOPS. From the first three columns in Fig. 5, the X and Y components spread to be donut shaped [Figs. 5(a) and 5(c)] from 10 lobes [Fig. 5(b)] by manipulating 2γ (i.e., -2ϑ) from 0 to $\pm\pi/2$. Keeping $\gamma = 0$, we observed that the 10 lobes in the X and Y components rotated by the angle of HWP (i.e., $\beta = 2\chi$) [Figs. 5(b) and 5(d)–5(f)]. The far-field distributions (Fig. 5) measured in the focal plane of sample 2 match well with the theoretically obtained far-field distribution [Fig. 4(a)].

To show the tight focusing property of the fifth-order HOPS beams, the size of each lobe in Figs. 5(b) and 5(d)–5(f) is quantitatively evaluated. Each lobe has a tiny lateral full width at half-maximum (FWHM) of 828 nm, which is 22% smaller than the diffraction limitation (1062 nm, 0.61λ/NA), which indicates that the tightly focused HOPS beams can be used for superresolution imaging and photolithography.

4.3 Generation of Tightly Focused 0-2 Order HyOPS Beams

We studied the metasurface sample 3 with a diameter of 4 mm in simulation and experiment for generating arbitrary focused

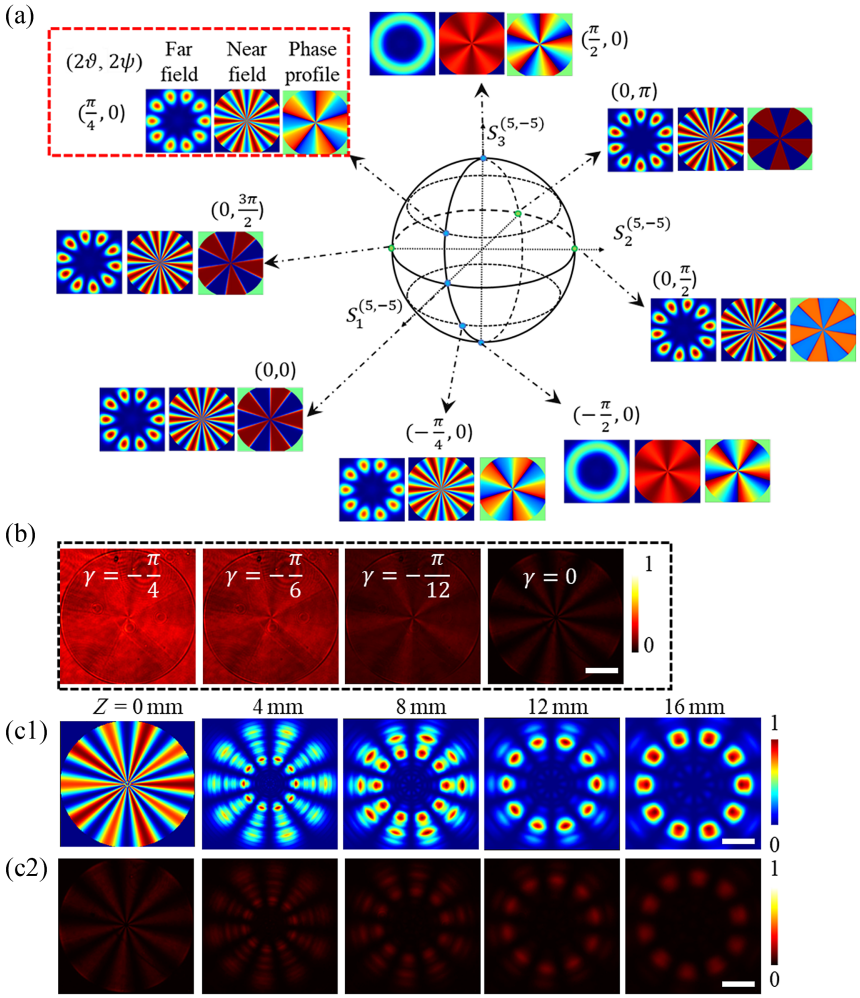

Fig. 4 (a) Simulated far-field, near-field, and phase profile distributions of the X component in the transmitted light beams over the target fifth-order HOPS by manipulating the position angles $(2\vartheta, 2\psi)$. (b) Measured near-field distribution of the X component. (c1) and (c2) The simulated and experimental results of the X component's propagation evolution from the metasurface ($Z = 0$ mm) to $Z = 16$ mm. Scale bars: 130 μm.

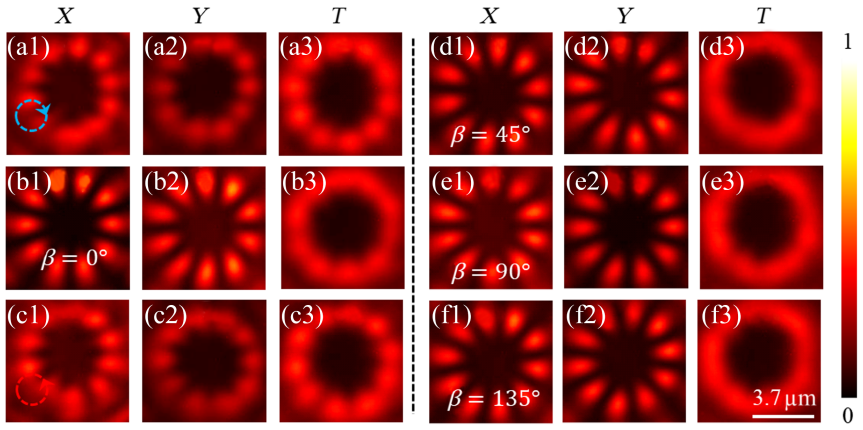

Fig. 5 Experimental results: controlled generation of tightly focused fifth-order HOPS beams (a1)–(c3) along its longitude line and (d1)–(f3) along its equator. The first and fourth columns are the X components in the total focal fields T (the third and sixth columns), and the second and fifth columns are the Y components.

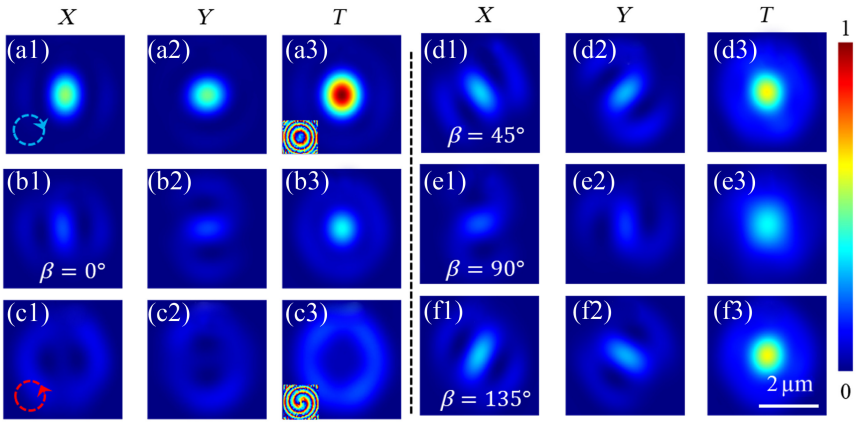

Fig. 6 Simulation results: controlled generation of 0-2 order HyOPS beams (a1)–(c3) along its longitudinal line and (d1)–(f3) along its equator. The first and fourth columns are the *X* components in the total focal fields *T* (the third and sixth columns), and the second and fifth columns are the *Y* components.

beams on the 0-2 order HyOPS. As shown in Fig. 1(c), from the northern pole to the southern pole along a latitude line, the topological charge (TC) gradually increases to 2 from 0. The beams on its equator are the first-order CVVBs with a TC of 1 [Eq. (12)]. It is first verified that the outgoing beams from the metasurface can be tuned from a scalar RCP (LG00, TC, $\ell = 0$) to a CVVB (TC, $\ell = 1$) and to a scalar LCP (LG00, TC, $\ell = 2$), with the incident laser beam being tuned from a scalar LCP to an LP and an RCP beam in simulation (the first three columns in Fig. 6). By rotating the polarization direction of the incident LP beam, the arbitrary first-order CVVBs (TC, $\ell = 1$) are generated via this metasurface (the last three columns in Fig. 6).

The LG00 focal point is measured to obtain the metasurface's NA under the LCP beam illumination. The FWHM of the LG00 focal point is measured to be 1060 nm [Fig. 7(c1)], demonstrating that the fabricated metasurface has an NA of 0.89. As the incident beam's polarization state changes from LCP to RCP, the focal point is tuned from a diffraction-limited LG00 spot [Fig. 7(a)] to an LG02 donut [Fig. 7(c)] along the 0-2 order HyOPS latitude line. We can see the intensity in the focal plane gradually spreads from the central area to the donut ring [Figs. 7(a)–7(c)], with the incident laser beam's polarization being tuned from LCP to RCP by rotating a QWP.

As predicted by Eq. (12) and simulation results in Fig. 6, we can experimentally generate arbitrary first-order CVVBs by manipulating the illumination light beam's polarization direction β and rotating the HWP [Figs. 7(b) and 7(d)–7(f)]. For $\beta = 0$, an azimuthal VVB (a special case of the CVVBs) is generated and is tightly focused. As a result, a focal point (FWHM = 870 nm), which is 18% smaller than the diffraction limitation (1062 nm, $0.61\lambda/\mathrm{NA}$), is obtained [Fig. 7(b)]. We also observed that the focal point's size goes up and its intensity goes down with the polarization direction changing from *X*-polarized ($\beta = 0$ deg) beam to *Y*-polarized beam ($\beta = 90$ deg). Furthermore, it is measured that the eight-shaped intensity distribution of the *X* components (the first and third columns in Fig. 7) and *Y* components rotates with the polarization direction β [Figs. 7(b1) and 7(d1)–7(f1)].

4.4 Generation of Tightly Focused 0-1 Order HyOPS Beams

The order (1) and topological charge (1) of the CVVBs generated by the 0-2 order HyOPS are integer values, and a super-resolution focal point beyond the diffraction limitation is obtained in both simulation and experiment. It is theoretically reported that there is a distinct focusing property between the CVVBs with the integer order/topological charge and fractional order/topological charge. We designed and fabricated sample 4 with a diameter of 4 mm to study the difference in the experiment. Sample 4 is studied in simulation (Fig. 8) and experiment (Fig. 9). According to Eq. (11), the topological charge carried by all VVBs on the 0-1 order HyOPS is fractional. Based on Eq. (12), the CVVBs represented by the 0-1 order HyOPS' equator have an order of 0.5 and a topological charge of 0.5.

We studied the tunability of the topological charge of the transmitted light beam by manipulating the illumination light beam's polarization state. With the illumination light beam tuned from LCP to RCP, the transmitted light beam is tuned from a diffraction-limited Gaussian spot [FWHM = 1060 nm, Figs. 8(a3) and 9(a3)] to an LG01donut [Figs. 8(c3) and 9(c3)]. Because the topological charge (1) carried by the southern pole of 0-1 order HyOPS is smaller than that (2) of the 0-2 order HyOPS, we observed that the radius of the central holes shown in Figs. 8(c3) and 9(c3) is smaller than that in Figs. 6(c3) and 7(c3).

Comparing the data in Secs. 4.3 and 4.4, we can see a clear difference in the intensity evolution along the longitude line of the 0-1 order and 0-2 order HyOPSs from the northern to southern poles. While the light energy spreads from a Gaussian solid point to a donut and keeps rotational symmetric for the 0-2 order HyOPS (Sec. 4.3), the light intensity maximum is offset from the optical axis, and intensity distribution becomes non-symmetric around the optical axis for the 0-1 order HyOPS (Sec. 4.4). Moreover, a nonaxial zero point appears in the focal field of arbitrary VVBs on the 0-1-order HyOPS, which arises from the superposition of the fractional vortex phase carried by the LCP and RCP components [Eq. (11)].

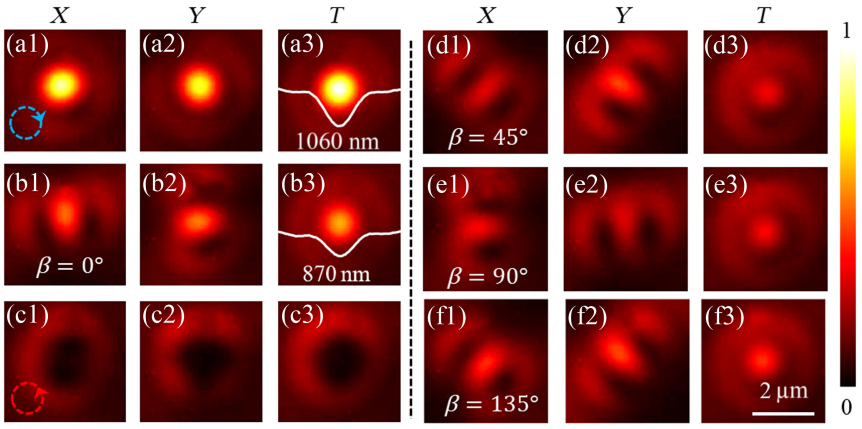

Fig. 7 Experimental results: controlled generation of 0-2 order HyOPS beams (a1)–(c3) along its longitudinal line and (d1)–(f3) along its equator. The first and fourth columns are the *X* components in the total focal fields *T* (the third and sixth columns), and the second and fifth columns are the *Y* components.

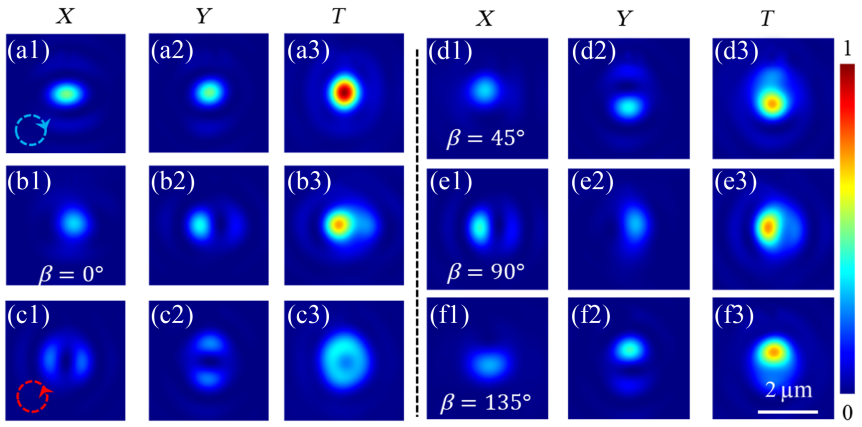

Fig. 8 Simulation results: controlled generation of 0-1 order HyOPS beams (a1)–(c3) along its longitudinal line and (d1)–(f3) along its equator. The first and fourth columns are the *X* components in the total focal fields *T* (the third and sixth columns), and the second and fifth columns are the *Y* components.

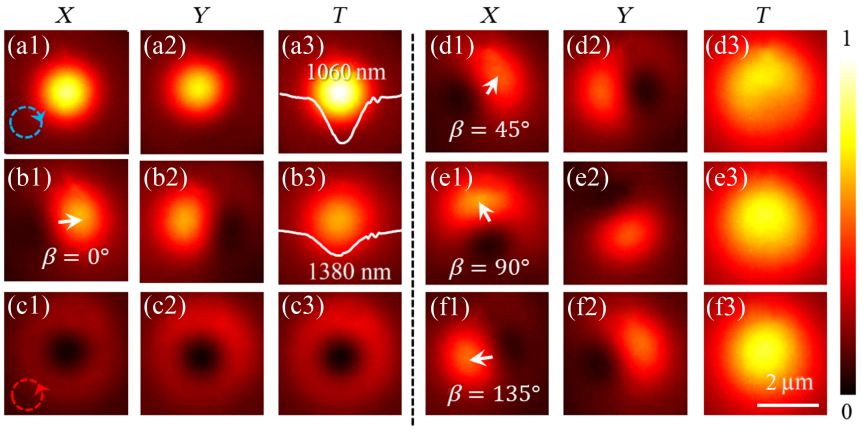

Fig. 9 Experimental results: controlled generation of 0-1 order HyOPS beams (a1)–(c3) along its longitudinal line and (d1)–(f3) along its equator. The first and fourth columns are the *X* components in the total focal fields *T* (the third and sixth columns), and the second and fifth columns are the *Y* components.

When sample 4 is illuminated by an LP light beam, the uniaxial symmetric property is distinct in the focal plane [Fig. 9(b)]. As a result, the FWHM of the total field [Fig. 9(b3)] is 1380 nm and larger than the diffraction limitation. By changing the LP direction β, the nonaxial maximum intensity [arrows in Figs. 9] and null intensity in X and Y components rotate around the optical axis. These experimental results in Fig. 9 match well with the simulation results in Fig. 8 and the reported theoretical results in Ref. 36. As far as we know, the tightly focusing properties of fractional VVBs and CVVBs are experimentally reported for the first time, highlighting our unified design framework's merit.

5 Conclusion and Discussion

A general design framework of the single-layer dielectric metasurface is proposed to generate arbitrary nonfocused/focused VVBs on the HOPS/HyOPS. The design framework is proposed by deriving the phase modulation mechanism of the single-layer dielectric metasurface via the Jones matrix and theoretically analyzing the connection between the HOPS and HyOPS. The controlled generation mechanism is illustrated based on the T-matrix method. Based on an orthogonal LP basis, the simultaneous modulation of local polarization direction and phase is obtained for the first time, to our knowledge, to analyze the controlled generation of cylindrical VVBs on the HOPS/HyOPS' equator. As a result, it can be determined that the vector order and topological charge of the cylindrical VVBs represented by the equator of M-N-order HyOPS are $(N-M)/2$ and $(N+M)/2$, respectively. When $M=-N$, the vector order and topological charge are N and zeros, which means that the beams represented by the equator of the N'th-order HOPS are N'th-order cylindrical vector beams without vortex phase.

We demonstrated four detailed proof-of-concept experiments to show the merit of our unified design framework. At first, the nonfocused and tightly focused (NA = 0.89) fifth-order HOPS beams are generated in both simulation and experiments to demonstrate HOPS beams' propagation and focusing properties. Then the tightly focused (NA = 0.89) 0-2 order and 0-1 order HyOPS beams are, respectively, generated via another two metasurface samples. In the experiment, we observed the super-resolution focusing performance of the first-order cylindrical vector vortex (topological charge is 1) beams on the 0-2 order HyOPS' equator and the different focusing properties of integer-order (0-2 order HyOPS equator beams) and fractional-order cylindrical vector vortex (0-1 order HyOPS equator beams) beams.

Based on the proposed unique design framework for generating arbitrary HOPS/HyOPS beams with a tailored focusing profile, we believe that this research could boost the metasurface's applications in multimode imaging, laser communication, structured optical tweezers, and the HOPS/HyOPS-beams-based metrology systems. It is well known that the imaging modes of an infinitely corrected microscope rely on the point spread function as well as the focal field's distribution of the objective lens, a multimode imaging system can be achieved by adopting a metasurface (e.g., the samples 2 to 4) with a polarization-controlled focal field. The HOPS/HyOPS beams have been regarded as high-potential candidates for achieving high-capacity laser communication and structured optical tweezers, and the high focusing of HOPS/HyOPS beams is of vital importance. Conventionally, the HOPS/HyOPS beams are first generated by a metasurface or SLM and then focused by a high-NA lens for the structured optical tweezers. In contrast, we demonstrated a more compact solution for these applications by integrating the generation and high focusing of HOPS/HyOPS beams into one single-layer metasurface via the proposed design framework. In addition, the metasurface-based compact generation of focused HOPS/HyOPS beams paves the way for developing a miniaturized and handheld precision metrology system. More importantly, the researchers on developing HOPS/HyOPS beams-based application systems have little knowledge of designing and fabricating a metasurface. We believe that this paper would reduce the barriers for them to generate arbitrary unfocused/focused HOPS/HyOPS beams via a single-layer dielectric metasurface.

Disclosures

The authors declare no conflicts of interest.

Code and Data Availability

All data in support of the findings of this paper are available within the article or as the Supplementary Material.

Acknowledgments

A PhD studentship from the Chinese Scholarship Council is acknowledged. This work was supported by the UK's Engineering and Physical Sciences Research Council (Grant Nos. EP/V000624/1, EP/X03495X/1, EP/X041166/1, and EP/T02643X/1) and the Royal Society (Grant No. RG\R2\232531).

References

1. C. He, Y. Shen, and A. Forbes, "Towards higher-dimensional structured light," *Light. Sci. Appl.* **11**, 205 (2022).
2. I. Nape et al., "Revealing the invariance of vectorial structured light in complex media," *Nat. Photonics* **16**, 538–546 (2022).
3. M. Liu et al., "Super-resolution optical microscopy using cylindrical vector beams," *Nanophotonics* **11**(15), 3395–3420 (2022).
4. E. Otte and C. Denz, "Optical trapping gets structure: structured light for advanced optical manipulation," *Appl. Phys. Rev.* **7**, 041308 (2020).
5. G. Kontenis et al., "Optical drills by dynamic high-order Bessel beam mixing," *Phys. Rev. Appl.* **17**, 034059 (2022).
6. Q. Zhan, "Cylindrical vector beams: from mathematical concepts to applications," *Adv. Opt. Photonics* **1**, 1–57 (2009).
7. G. Milione et al., "Higher-order Poincaré sphere, Stokes parameters, and the angular momentum of light," *Phys. Rev. Lett.* **107**, 053601 (2011).
8. X. Yi et al, "Hybrid-order Poincaré sphere," *Phys. Rev. A* **91**(2), 023801 (2015).
9. D. Lin et al., "Reconfigurable structured light generation in a multicore fibre amplifier," *Nat. Commun.* **11**(1), 3986 (2020).
10. Y. Shen et al., "SU(2) Poincaré sphere: a generalized representation for multidimensional structured light," *Phys. Rev. A* **102**, 031501 (2020).
11. Y. Shen et al., "Optical vortices 30 years on: OAM manipulation from topological charge to multiple singularities," *Light. Sci. Appl.* **8**, 90 (2019).
12. Y. Shen et al., "Structured ray-wave vector vortex beams in multiple degrees of freedom from a laser," *Optica* **7**(7), 820 (2020).
13. Z. Wan et al., "Ultra-degree-of-freedom structured light for ultra-capacity information carriers," *ACS Photonics* **10**, 2149 (2023).
14. N. Yu et al., "Light propagation with phase discontinuities: generalized laws of reflection and refraction," *Science* **334**, 333–337 (2011).

15. M. K. Chen et al., "Principles, functions, and applications of optical meta-lens," *Adv. Opt. Mater.* **9**(4), 2001414 (2021).
16. W. T. Chen et al., "Flat optics with dispersion-engineered metasurfaces," *Nat. Rev. Mater.* **5**(8), 604–620 (2020).
17. S. M. Kamali et al., "A review of dielectric optical metasurfaces for wavefront control," *Nanophotonics* **7**(6), 1041–1068 (2018).
18. A. H. Dorrah et al., "Metasurface optics for on-demand polarization transformations along the optical path," *Nat. Photonics* **15**, 287–296 (2021).
19. H. Ren et al., "Complex-amplitude metasurface-based orbital angular momentum holography in momentum space," *Nat. Nanotechnol.* **15**, 948–955 (2020).
20. Y. Y. Xie et al., "Metasurface-integrated vertical cavity surface-emitting lasers for programmable directional lasing emissions," *Nat. Nanotechnol.* **15**, 125–130 (2020).
21. D. Wen and K. B. Crozier, "Metasurfaces 2.0: laser-integrated and with vector field control," *APL Photonics* **6**(8), 080902 (2021).
22. H. Sroor et al., "Generation of arbitrary higher order Poincaré beams from a visible metasurface laser," *Proc. SPIE* **11266**, 112660L (2020).
23. X. Zeng et al., "Arbitrary manipulations of focused higher-order Poincaré beams by a Fresnel zone metasurface with alternate binary geometric and propagation phases," *Photonics Res.* **10**, 1117–1126 (2022).
24. D. Wen et al., "Broadband multichannel cylindrical vector beam generation by a single metasurface," *Laser Photonics Rev.* **16**, 2200206 (2022).
25. Y. Bao, J. Ni, and C.-W. Qiu, "A minimalist single-layer metasurface for arbitrary and full control of vector vortex beams," *Adv. Mater.* **32**(6), 1905659 (2020).
26. S. Wang et al., "Arbitrary polarization conversion dichroism metasurfaces for all-in-one full Poincaré sphere polarizers," *Light Sci. Appl.* **10**, 24 (2021).
27. G. Li et al., "Spin-enabled plasmonic metasurfaces for manipulating orbital angular momentum of light," *Nano Lett.* **13**(9), 4148–4151 (2013).
28. H. Li et al., "Polarization detection of terahertz waves using all-silicon metasurfaces with tightly focusing behavior," *Laser Photonics Rev.* **17**, 2300428 (2023).
29. J. Ji et al., "Metasurface-enabled on-chip manipulation of higher-order Poincaré sphere beams," *Nano Lett.* **23**(7), 2750–2757 (2023).
30. S. Wang et al., "Metasurface-based solid Poincaré sphere polarizer," *Phys. Rev. Lett.* **130**(12), 123801 (2023).
31. R. C. Devlin et al., "Arbitrary spin-to-orbital angular momentum conversion of light," *Science* **358**, 896–901 (2017).
32. J. Liu et al., "Generation of arbitrary cylindrical vector vortex beams with cross-polarized modulation," *Results Phys.* **19**, 103455 (2020).
33. J. Yang et al., "Generation of arbitrary vector Bessel beams on higher-order Poincaré spheres with an all-dielectric metasurface," *Phys. Rev. A* **106**(2), 023520 (2022).
34. G. Cao et al., "Infrared metasurface-enabled compact polarization nanodevices," *Mater. Today* **50**, 499–515 (2021).
35. Z. Feng et al., "Perfecting and extending the near-infrared imaging window," *Light Sci. Appl.* **10**, 197 (2021).
36. Y. Miao et al., "Tight-focusing properties of propagable fractional-order vector vortex beams," *J. Opt. Soc. Am. B* **40**(5), 1113–1120 (2023).

Biographies of the authors are not available.